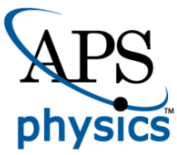

Impact of confined geometries on hopping and trapping of motile bacteria in porous media

Lazaro J. Perez, Tapomoy Bhattacharjee, Sujit S. Datta, Rishi Parashar, and Nicole L. Sund

Phys. Rev. E **103**, 012611 — Published 25 January 2021

DOI: 10.1103/PhysRevE.103.012611

Impact of confined geometries on hopping and trapping of motile bacteria in porous media

Lazaro J. Perez*
Division of Hydrologic Sciences,
Desert Research Institute, Reno, NV, USA

Tapomoy Bhattacharjee
The Andlinger Center for Energy and the Environment,
Princeton University, Princeton, NJ, USA

Sujit S. Datta
Department of Chemical and Biological Engineering,
Princeton University, Princeton, NJ, USA

Rishi Parashar and Nicole L. Sund
Division of Hydrologic Sciences,
Desert Research Institute, Reno, NV, USA

We use a random walk particle-tracking (RWPT) approach to elucidate the impact of porous media confinement and cell-cell interactions on bacterial transport. The model employs stochastic alternating motility states consisting of hopping movement and trapping re-orientation. The stochastic motility patterns are defined based on direct visualization of individual trajectory data. We validate our model against experimental data, at single cell resolution, of bacterial *E. coli* motion in 3D confined porous media. Results show that the model is able to efficiently simulate the spreading dynamics of motile bacteria as it captures the impact of cell-cell interaction and pore confinement, which marks the transition to a late time subdiffusive regime. Furthermore, the model is able to qualitatively reproduce the observed directional persistence. Our RWPT model constitutes a mesh-less simple method which is easy to implement and does not invoke *ad-hoc* assumptions but represents the basis for a multi-scale approach to the study of bacterial dispersal in porous systems.

I. INTRODUCTION

Bacterial migration through heterogeneous porous media is important for a wide range of processes, such as bioremediation, biofilm formation and anticancer drug delivery [1–4]. In natural environments, bacteria employ diverse movement modalities while navigating through porous media that characterize their migration [5]. Motility is the capability of an organism to spontaneously perform independent moves, which enables bacteria to explore space and other resources and to forage or disperse. Bacterial transport, therefore, encapsulates processes that act across multiple spatial and temporal scales, that are not only key for innovative applications but also for their growth and interactions with the physical environment [6].

Many bacteria actively swim via flagella, or twitch over surfaces. Disregarding the way they move, most observations of bacterial motility are undertaken in bulk fluid to avoid artifacts arising from surface and cell-cell interactions [7–9]. As a result, little is known about the effects that confined porous spaces have on motility. A common assumption is that bacteria perform linear short movements caused by collisions with the medium solid boundaries. Interaction between cells and cell-boundary collisions are thought to reorient cells, similar to tumbles for *E. coli* [1] or flicks and reversals for *V. Alginolyticus* [10], leading to a decreased diffusivity.

Traditionally, modeling the motility of many bacteria via flagella movement in aqueous systems has been conceptualized using two alternating movement periods due to the stochastic nature of bacterial motion [11, 12]. Models assume that bacteria movement is composed of two modes: runs consisting of a linear straight movement followed by tumbles consisting of random changes in direction that mimic interaction between cells and collisions with obstacles [11, 13–15]. Other methods may include particle tracking techniques that rely on image segmentation algorithms [16], fitting cells path curve to an evolving model [17], as well as non-Poissonian run-and-tumble patterns [18] suggesting that at least one of the steps in the regulation of reversal is thermodynamically irreversible.

Numerical observations assume that cells' movement is a stochastic process [10, 11, 19], and the derivation of its descriptive parameters requires clear discrimination of the stochastic patterns that relies on the rules that dictate random models. Random walk particle tracking

* lazaro.perez@dri.edu

(RWPT) approaches have been long used to model cell migration [17, 20, 21]. Although this approach provides an expression for modeling cell migration, in most cases, the movement of individual cells cannot be attributed to a simple random walk behavior. Recent mathematical and modelling works have used modified random walk models by introducing repelling, reflecting, or absorbing barriers, to account for bacterial interactions with solid boundaries and between cells [22–25]. While others intersperse two turning events in strictly alternating order to reproduce cell swimming directions. Despite some differences in the migration process modeled, these models commonly obviate transient short time dynamics in motility states; or how the diffusive dynamics depend on the run and tumble velocities and the switching probabilities between the two states.

A detailed mathematical analysis of the motility properties of the micro-swimmers is essential for prediction of microbial dispersal under realistic conditions. Based on existing theories [26], we develop a two-state RWPT model that mimics and describes the hopping and trapping experimental dynamics reported in [27]. The model uses stochastic alternating motility states derived from direct inspection of cells trajectory data. The model highlights the coupling between cell's direction and speed in confined geometries. We successfully capture the intermediate and long term spreading of *E. coli* in a confined porous medium.

The paper is organized as follows. Section II describes the experimental and data analysis methodology, as well as the RWPT approach. Section III discusses the motility patterns observed in the experimental visualization, and presents the modeling results. Finally, we conclude and give an outlook on further expansion of our model in Section IV.

II. METHODOLOGY

In the following, we first summarize the experimental setup presented in Bhattacharjee and Datta [27], whose data we use to evaluate our model's ability to reproduce the observed motility patterns. Then we recall the approach to analyze bacterial migration and discriminate between motility states. Finally, we present a numerical model to reproduce the observed findings in the experiment.

A. Experimental data

As detailed in [27, 28], we use confocal microscopy to visualize fluorescent *E. coli* (strain W3110) homogeneously dispersed in transparent, jammed packings of hydrogel particles. The packings act as solid matrices with macroscopic interparticle pores of average size $\lambda = 1.9$ or 3.6 μm that the cells can swim through. The internal mesh size of each hydrogel particle is much smaller than the individual cells, but large enough to allow unimpeded transport of nutrients and oxygen, giving rise to homogeneous nutrient conditions throughout the packing.

In each experiment, we disperse the cells within 4 mL of a jammed hydrogel packing at 6×10^4 vol%, sufficiently dilute to minimize intercellular interactions, crossing of cellular trajectories, and any influence of nutrient consumption. We confine each medium inside a sealed glass-bottom petri dish, with a packing height $\sim$1 cm, and add an overlying thin layer of 750 μL liquid medium to prevent evaporation. We then use a Nikon A1R+ inverted laser-scanning confocal microscope with a temperature-controlled stage at 30°C to capture fluorescence images every 69 ms from an optical slice of 79 μm thickness. The sampling interval of 69 ms is sufficiently fast to uniquely identify cells, since they do not move more than approximately three cell body lengths between consecutive time points, while minimizing photobleaching of the fluorescent signal. Further, to avoid any boundary effects, all images are captured at least 100 μm from the bottom of the container. Using this platform, we monitor bacterial motion through the pore space, acquiring projected two-dimensional (2D) movies within the porous media. To track the individual cells, we then use a custom MATLAB script developed in-house to identify and track each cell center using a peak finding function with subpixel precision using the classic Crocker-Grier algorithm [29]. We track cell motion for at least 10s, five times larger than the unconfined run duration but over five times shorter than the cell division time, and focus our analysis on cells that exhibit motility within the tracking time.

This platform enabled us discover a new mode of motility exhibited by *E. coli* in porous media [27]. Instead of moving via run-and-tumble dynamics with truncated runs, as is often assumed, we found that the cells are intermittently and transiently trapped in tight spots as they move through the pore space. When a cell is trapped, it constantly reorients its body until it is able to escape; it then moves in a directed path through the pore space, a process we call hopping, until it again encounters a trap.

B. Trajectory analysis

In order to perform behavior discrimination, several quantitative features have been proposed such as average velocity [1], moving average of incremental displacements [15], turning events [30, 31], among others. Here, we use a moving average of incremental displacements (MAID) to distinguish between motility states in the extracted bacterial trajectories from [27]. MAID has performed well in discriminating hopping and trapping modes compared to other features in a limited number of bacterial trajectories [15].

Differences in bacterial motility modes lead to significant effects on their migration. For instance, bacterial trapping produces a significant decrease in effec-

tive swimming speed, and thus a decrease in incremental displacement is expected. By contrast, the incremental displacements during hopping mode increases [1, 15]. Therefore, incremental displacements, defined as the Euclidean distance between two consecutive points in a cell trajectory, can be used quantitatively to discriminate between hopping and trapping states. In our case, hopping and trapping states were identified by means of bacterial speed as the threshold parameter before MAID is applied. The moving average of the incremental displacements reduces noise effects in the incremental displacements analysis given as

$$\kappa_t = \frac{1}{w} \sum_{i=-(w-1)/2}^{(w-1)/2} d_{t+i}, \tag{1}$$

where w is the window size for calculating the moving average of the incremental distance κ at time t, and d_{t+i} is the Euclidean distance between consecutive time steps in a cell trajectory. We extract the motility parameters that govern bacterial transport separately for hopping and trapping modes to characterize our mathematical model. In summary, when a cell speed is above the ensemble trajectory average speed, the cell is considered to be in a hop. On the other hand, if the cell speed is below the ensemble trajectory average speed, the cell is regarded to be in a trapping state. We chose this specific parameter value because it provides a good comparison between the obtained classification of hopping and trapping, and the traditional runs and tumbles [15, 31–33]. We performed a sensitivity analysis to other criteria to discriminate between motility states (e.g., deviation angle variance) and the resulting statistical characteristics of the analyzed trajectories were robust to variations as large as $\sim 10\%$. We determined the marginal distribution of velocities for hopping and trapping modes from the trajectory analysis [15] to analyze and understand the pore-scale cell motion which constitutes a central part in the developed model. The change in the trajectory direction or body orientation, θ, with respect to the arrival direction in a given time step is computed from the bearing angle α from $\mathbf{x}(t)$ to $\mathbf{x}(t+\Delta t)$ as the angle measured in the clockwise direction from the line segment to the horizontal line,

$$\tan\alpha(t) = \frac{y(t+\Delta t) - y(t)}{x(t+\Delta t) - x(t)}, \tag{2}$$

where $\mathbf{x}(t) = [x(t), y(t)]$ is the position of the cell at time t and Δt is the experimental sampling interval. Figure 1 shows the trajectory of a cell during two successive steps and how we extract α and θ from the pathways of each cell obtained from the particle tracking module.

Our emphasis is on the comparison between simulations and experimental data, therefore we assess the accuracy of our numerical model based on the computed the mean squared displacement (MSD) given as

$$\mathrm{MSD}(\mathcal{S}) = \langle \mid \mathbf{x}(t+\mathcal{S}) - \mathbf{x}(t) \mid^2 \rangle \tag{3}$$

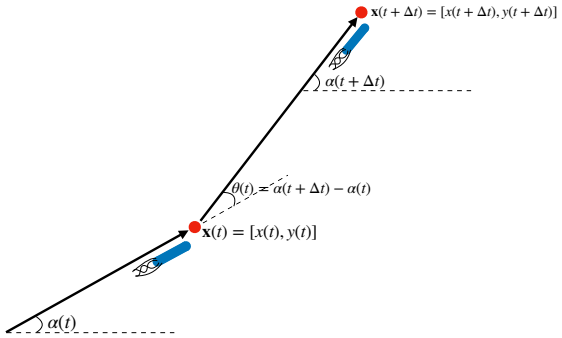

FIG. 1. Illustration of the trajectory of a cell during two successive steps.

where $\mid \mathbf{x}(t+\mathcal{S}) - \mathbf{x}(t) \mid$ is the particle displacement between two time points, t denotes the absolute time while $\mathcal{S}$ is the so-called lag time [1]. Additional information about the experimentally observed bacterial behavior can be extracted from the normalized velocity autocorrelation function C

$$C(\mathcal{S}) = \frac{\langle \mathbf{v}(t+\mathcal{S}) \cdot \mathbf{v}(t) \rangle}{\langle \mathbf{v}^2(t) \rangle}, \tag{4}$$

where $\mathbf{v}$ stands for velocity. C can also be found by double differentiation of the MSD.

C. Mathematical model

To describe quantitatively the dispersal dynamics that bacteria exhibit in [27], we propose the following random walk model,

$$\mathbf{x}(t+\Delta t) = \mathbf{x}(t) + \mathbf{v_m}(t)\Delta t + \sqrt{2D\Delta t}\boldsymbol{\xi}(t), \tag{5}$$

where $\mathbf{v_m}$ is the motile velocity vector, and the diffusion coefficient D is approximated from the experimental data as

$$D = \frac{\langle [\mathbf{x}(t_m) - \mathbf{x}(t_m - \mathcal{S})]^2 \rangle}{6t_m}, \tag{6}$$

where t_m is the maximum observation time. D varies from 0.53 μm^2/s for $\lambda = 1.9\mu$m to 5.71 μm^2/s for $\lambda = 3.6\mu$m . We substitute a shifted and scaled uniform $[0,1]$ random variable $\sqrt{24D\Delta t}(\mathbf{U}(0,1) - 1/2)$ for the last term where $\mathbf{U}(0,1)$ is a vector of independent and identically distributed uniform random variables between 0 and 1 [34, 35]. This choice avoids the costly numerical generation of Gaussian random numbers. The central limit theorem guarantees that the sum of random displacements is again Gaussian. Each particle represents a single cell that moves with velocity $\mathbf{v_m}(t) \sim v_m(t)\mathbf{e}(t)$, where the subscript m stands for motility mode. The

speed $v_m(t)$ is the velocity of the cell and the unit vector $\mathbf{e}(t)$ denotes the direction of propagation at time t. The velocity magnitude and direction is simulated according to

$$\mathbf{v_m}(t) = v_m(t) \begin{pmatrix} \cos(\theta_m(t)) \\ \sin(\theta_m(t)) \end{pmatrix}, \tag{7}$$

where $\theta_m(t)$ is randomly chosen according to the turning-angle distribution $p_h(\theta)$ or $p_t(\theta)$ in the hopping or trapping state, respectively. While the speed $v_m(t)$ is chosen from a marginal velocity distribution that depends on the θ chosen in each motility mode. This $v_m(t)$ selection preserves the correlation between θ and v_m extracted from the trajectory analysis. We use the methodology presented in [36, 37] as sampling method to select θ_m and v_m from their known distributions.

The transitions between the motility states are determined based on the probability distributions obtained from the observed experimental trajectories. We found that the observed duration distribution of staying in the hopping state is well fitted by an exponential distribution; moreover, while the observed duration distribution of staying in the trapping state shows a long non-exponential tail, an exponential distribution provides a reasonable approximation for our computations. These findings have been observed in other *E. coli* experiments [5, 33, 38]. In our case, hopping times are approximated to be exponentially distributed with a mean hopping time τ_h, thus we use a hopping transition probability of the form

$$P(t < t + \Delta t) \sim e^{-(t-t_0)/\tau_h}, \tag{8}$$

where $t - t_0$ is the time passed from the previous change of state. Equation (8) describes the hopping probability, the trapping transition probability is analogous. Note that the probability of starting the motion in the hop or trap phase is denoted by P_0^h and P_0^t, respectively with

$$P_0^t = 1 - P_0^h. \tag{9}$$

The choice of an initial fixed hop probability [39] for all the particles showed no significant impact on the results here. The occurrence of a motility mode transition event is determined through a Bernoulli trial based on the transition probability (8).

In our numerical setup, the bacterial transport problem is solved with the RWPT simulator described (5). As the initial condition for simulations of both pore length experiments analyzed, we consider uniform areal distributions of particles from $[10, 120]$ μm and $[5, 70]$ μm, in x and y coordinates respectively. We implement bacterial confinement and collective dynamics assuming physical interaction between swimmers. When a particle is in hopping mode and closer than a cell body length, $\gamma = 2\mu$m, to another particle, its motility mode changes to trapping mode with $P = 1$, as a result of the collision [21, 24, 33, 40].

III. RESULTS

In the following, we study the transport dynamics of the experimental analysis in terms of the hopping and trapping discrimination for bacterial motility states. First, we describe the motility patterns for the evaluated bacterial states observed in the experimental visualization, which are the building blocks of the mathematical model presented in the previous section.

A. Motility patterns

We analyzed 41 cell trajectories with an average length of 12.42 s following the procedure detailed in the previous section. A typical trajectory is shown in Figure 2 (top plot), with the starting and final points respectively indicated with blue and yellow marks. The corresponding color-coded MAID plot against time in Figure 2 (lower plot) shows hopping and trapping discrimination based on the normalized ensemble mean incremental displacement, or in other words, the cells' ensemble mean velocity. Segments below 1 are identified as trapping states, while segments above the normalized threshold indicates that the cells are in hopping mode. As for window sizes in MAID features, w values of 5 to 21 were tested to illustrate the impact of the w value in the results to avoid artificial smoothing from higher w values. Results of this analysis show that $w = 9$ provides the best result in differentiating the hopping and trapping modes. Nonetheless, a window size of 21 (black solid line in Figure 2 lower plot), which implies a higher smoothing degree, provides optimal results in reducing noise without losing relevant information for bacterial motility state discrimination. The methodology, thus, mitigates the error propagation in the evaluation of the state discrimination in noisy data by optimizing bacterial motility data and avoiding visual calibrated motility state discrimination [33] from the empirical data.

Classical bacterial transport models fitted bacteria orientation angles undergoing run-and-tumble cycles using uniform distributions [41]. Experimentally, this means that, when a cell swims around rounded obstacles over a long enough time, the probability density function of θ should be uniform as it eventually samples all values of the cell body orientation angle (θ) within the plane of that surface with equal probability. This is also true for the overall orientation angles of an entire population of bacteria, as long as the cell trajectories are independent and interactions between trajectories (such as cell-collisions or hydrodynamic interactions) are random with no long-range correlations or event memory. This traditional notion changes in presence of chemical gradients, medium confinement, or flow [15, 27, 31, 42]. The results of θ orientation angle distribution from the experimental $\lambda = 1.9\,\mu$m shown in Figure 3 suggest straight hops and reverse turns in trapping mode, which is consistent with the run-reverse concept due to flagella rotation [5, 43].

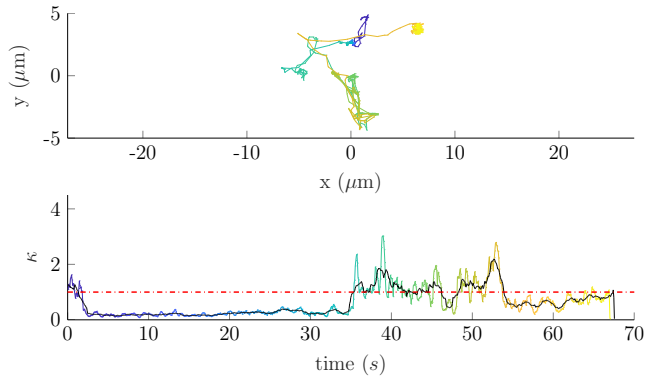

FIG. 2. Top: Trajectory of one cell. Bottom: Normalized MAID in which the color coded line shows initial position (blue) and final position (yellow) in the cell trajectory. The red dashed-dotted line delineates hopping from trapping mode. The black solid line corresponds to the MAID with a higher value of w.

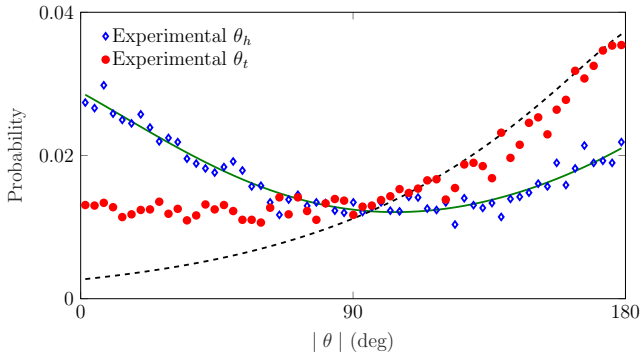

FIG. 3. Turn-angle distributions of the hopping (blue diamonds) and trapping (red dots) mode from smallest pore size (1.9 μm) in the experimental data and their fitted distributions (solid and dashed lines).

We observe that key difference between hopping and trapping is the ability of the cell to maintain its direction of motion during the course of a hop, while when trapped, the cell reverses its orientation which allows bacteria to escape bead traps by reversing their swim [43–45]. This feature sheds lights over the classical notion that broadly distributed angles for trapping mode indicates that their motion is uniform randomly oriented. Therefore, angular distributions in different motility modes cannot be ignored as they provide information on bacterial swimming strategy. The turn-angle distribution for both modes is bimodal with higher peaks near lower and higher values of | θ |. The distributions parameters, $\mu_h = [0.02\pi\ 0.88\pi]$ and $\mu_t = [-0.94\pi\ 0.89\pi]$, while σ_h and σ_t are [0.69 0.94] and [0.85 0.85] respectively, were found by fitting a Gaussian mixture model to data [46]. The bimodal distribution in turn-angle distributions indicates that when a cell chooses a new direction, is most likely to choose a new direction not very different or opposite from the previous

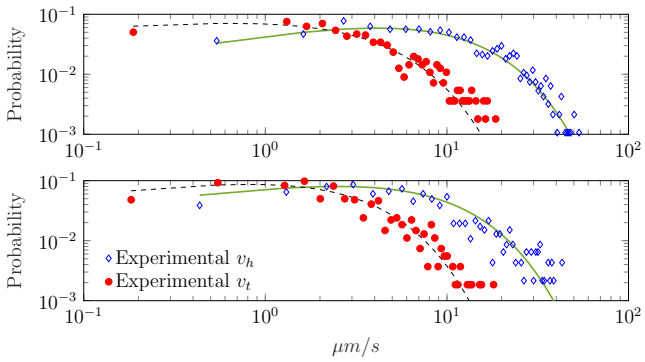

FIG. 4. Marginal velocity distribution for hopping (blue squares) and trapping (red dots) states from the smallest pore size (λ = 1.9 m) in experimental data and their fitted gamma distribution (solid and dashed lines respectively) for | θ |= [0, 10) (upper plot), and | θ |= [60, 70) (lower plot).

direction. This distribution is qualitatively similar to the reported for *E. coli* strain AW405 [47] and O157:H7 [48]; and for *Pseudomonas putida* [49, 50]. We find similar behavior for λ = 3.6 μm, thus we omit these data here and focus on the small pore size case.

Figure 4 shows the marginal velocity distributions from experimental data for $\lambda = 1.9\,\mu$m for two | θ | ranges. We found that the gamma distribution is the continuous distribution that best fit the experimental marginal velocity distributions for hopping and trapping modes (Figure 4). The gamma fitted distribution shows smaller root mean square error than other continuous distributions (log-normal, beta, generalized extreme value) that were tested. This result is the one expected for motile bacteria and suggests signs of enhanced transport processes over a scale larger than the pore size [15, 51]. It can be observed in Figure 4 that, as it is expected, the hopping state marginal distribution is slightly shifted to higher values for lower | θ | ranges and thus shows higher mean velocity $\bar{v}_{h,|\theta|=[0,10)}$ =12.33 μm/s (Figure (4 upper plot) than for higher | θ | ranges where $\bar{v}_{h,|\theta|=[60,70)}$ =9.16 μm/s (Figure (4 lower plot). The overall mean velocity for hopping state is $\bar{v}_h = 9.26\,\mu$m/s. The k and β parameters for the fitted gamma distributions for the hopping state showed variations such as $1.31 < k < 1.77$ and $4.01 < \beta < 8.54$. The trapping state marginal distributions display small variations for the different | θ | ranges showing the highest $\bar{v}_t$ =3.87 μm/s (k = 1.12 and β = 3.53) for | θ |= [10, 20); and lowest $\bar{v}_t$ =2.95 μm/s (k = 1.42 and β = 2.14) for | θ |= [120, 130), with an overall $\bar{v}_t = 3.22\,\mu$m/s.

The distributions of hop and trapping times are shown in Figure 5 where both modes are well fit by exponential distributions. Note that while there is some deviation in the tail of the trapping distribution (consistent with a power law [28]), the exponential fit provides a good first approximation. The mean hop time τ_h is given by the average value of the experimentally derived hop times, τ_h = 0.926s for $\lambda = 1.9\,\mu$m and τ_h = 0.804s for

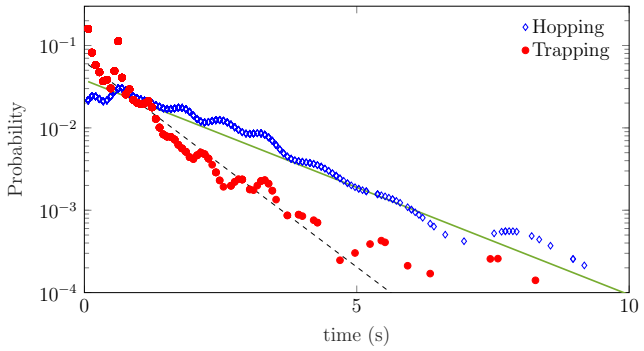

FIG. 5. Experimental distribution of duration of staying in hopping (blue diamonds) and trapping (red dots) mode and best fitting exponential distributions (green solid and black dashed lines).

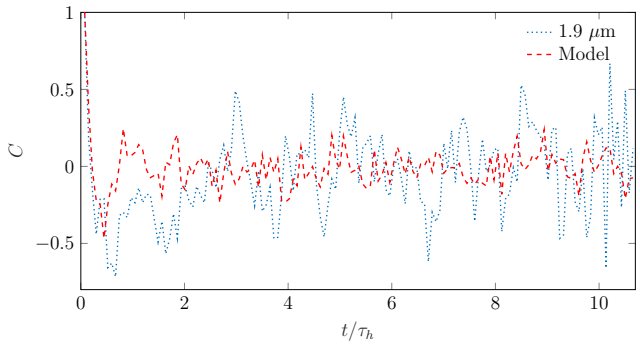

FIG. 6. Normalized experimental (blue dotted line) and model (red dashed line) velocity autocorrelation function plotted as function of dimensionless time t/τ_h.

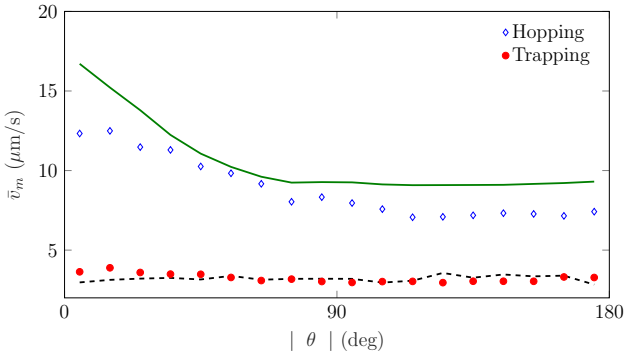

FIG. 7. Bacterial directional persistence in terms of different turning-angles ranges in $\lambda = 1.9\,\mu$m for hopping and trapping modes. Experimental and modeling results are shown in symbols and lines, respectively.

$\lambda = 3.6\,\mu$m. The lower value of τ_h for the greatest λ is attributed to higher frequencies of short hops [31]. On the other hand, the mean trapping time τ_t for $\lambda = 1.9$ and $\lambda = 3.6\,\mu$m are 0.44 and 0.42 s respectively. The exponential distribution is a simplifying assumption, which is, however, crucial for the modeling calculations.

B. Model comparison to experimental results

Based on the information extracted from the trajectory analysis, we simulate 5000 bacterial trajectories in the absence of chemotaxis using the random walk algorithm presented above. We validate the model against the experimental results [27].

Results of the computed velocity autocorrelation from the simulation and experimental data are shown in Figure 6. Time is made dimensionless by considering $t' = t/t_h$. For simplicity of notation, we omit the primes in the following. We find that the RWPT model provides a good description of the experimental velocity autocorrelation function. In particular, the model captures the shape of the experimental velocity autocorrelation function including the reproduction of the negative dip. This further justifies that the RWPT model used is appropriate to describe the motility patterns of *E. coli* in a confined geometry. We hypothesize that the quick decay and negative peak observed in C is due to pore confinement. This observation is supported by direct inspection of individual trajectory data. A clear example of this is inferred from the lower plot in Figure 2, where the plot of κ shows that the cell starts in hopping mode but changes its motility mode to trapping at $t < \tau_h$. Traditionally, this behavior in C has been described as the preconfined regime in RWPT models in confined geometries [21, 52, 53].

We now discuss the model's ability to reproduce bacterial directional persistence to determine whether turning angle ranges of the bacterial population affect the observed speed. We split up our data set of 10356 hopping and 13086 trapping speeds for $\lambda = 1.9\,\mu$m to create separate velocity distributions for 18 different turning angle ranges. Please note that for our simulation model we fit the gamma distribution as explained in the previous section to the velocities distributions. Figure 7 shows the mean instant velocity of each motility mode for different $|\,\theta\,|$ ranges. We find directional persistence in experimental data in hopping mode, as results indicate that turning angles ranges [0,10) and [10,20) show higher mean velocities than the rest of $|\,\theta\,|$ ranges. These results support the idea that higher velocities correspond to straight hops [27, 47], and thus coupling between v_h and $|\,\theta\,|$. At higher $|\,\theta\,|$ range intervals, we observe a decrease in mean velocities in hops, which indicates that when cells performs high angle turns in hopping mode they reduce their instant velocity, and that hops after cell reorientation are smaller than the bacterial population mean. The model shows higher average swimming speeds ($\bar{v}_m$) in hopping mode. The discrepancy between experimental and model observations is attributed to a more broad swimming speed sampling around the mean in the experimental observations. Note that model results for hopping approach the reported experimental $\bar{v}_h$ after $\bar{\theta}_h$. On the other hand, Figure 7 shows that the

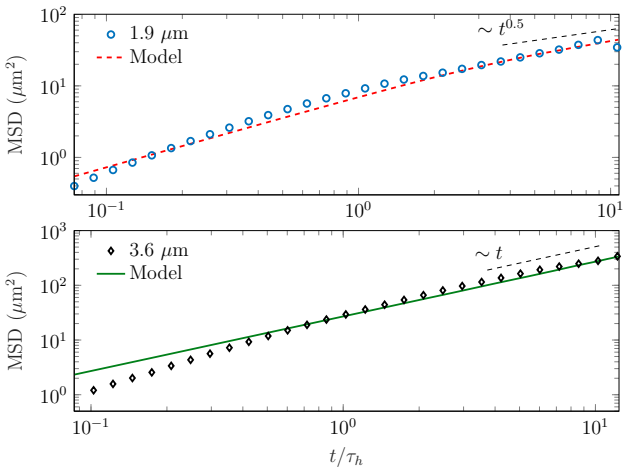

FIG. 8. Evolution of the mean squared displacement (MSD) computed for different pore sizes, 1.9 μm (upper plot) and 3.6 μm (lower plot). Experimental MSD is shown in symbols in both plots, and the RWPT simulation results for 1.9 μm (red dashed line in upper plot) and 3.6 μm (green solid line in lower plot).

trapping mode exhibits a more stable range of mean instant velocities around the reported $\bar{v}_t$. We find good agreement between model and experimental evidence. Our findings shed light on the mechanisms underlying cell reorientation as *E. coli* swimming is driven by the rotation of flagella. The resulting reorientation is commonly modeled using rotational diffusion, which implies a persistence that decreases exponentially with trapping duration [30, 32] that fails to capture bacterial dispersion at late times. Moreover, the changes in mean instant velocities according to $\mid \theta \mid$ that we observe do not result from differences in trapping duration. Further imaging studies of swimming cells with labelled flagella may be able to clarify this observation.

Results of the computed MSD from both the experimental and the simulated trajectories are presented in Figure 8. At early times, we observe that experimental MSD for both pore lengths experiments, $t \ll \tau_h$, shows superdiffusive regime which our model is not able to capture as the MSD from simulations exhibits diffusive behavior at early times. The discrepancy between model and experiment can be attributed to the use of the approximated D coefficient following (6) in the diffusive step in (5), which does not quantify properly spreading at $t \ll \tau_h$. As t approaches τ_h, a transition to a diffusive regime occurs. The transition happens because cell-cell and cell-obstacle interaction effects increase which affects bacterial step lengths and thus, their motility behavior. Please note that the duration of superdiffusive motion decreases as pore confinement increases (Figure 8). This is observed by direct comparison of the experimental MSDs for the two different pore sizes, which reveals that the superdiffusive behavior in $\lambda = 3.6$ (Figure 8 lower plot) and $\lambda = 1.9\,\mu$m (Figure 8 upper plot) lasts $t = 0.5\tau_h$ and $t = 0.15\tau_h$, respectively. There is good agreement between experimental and model results. At late times, the emergence of a subdiffusive regime is observed in the case of $\lambda = 1.9\,\mu$m, where bacterial confinement leads to non-linear behavior, which is consistent with previous observations [54]. This subdiffusive phenomenon is delayed in the larger pore size but is also expected for $t \gg 10$. Note that we restricted our experimental analysis to 10 s because of noisy data at greater times. The late time subdiffusive regime is reflected in the evolution of the experimental MSD, which grows as $\sim t^{1/2}$, shown in Figure 8 upper plot. The non-linear increase of the MSD is well described by the RWPT model as it captures interaction between cells and pore confinement which affects bacterial motility. In addition, the late time agreement between model and experimental data in Figure 8 (upper plot) stems from the correct characterization of the experimental directional persistence in trapping mode as subdiffusive dynamics are commonly attributed to trapping states [54, 55]. Analysis of MSD of individual cells for $\lambda = 1.9\,\mu$m reveals that subdiffusive behavior may be transient and collapses back to normal diffusion in some cells. This effect is masked in averaging. The transient subdiffusive behavior have been observed in the experimental cases of obstructed diffusion [56] and computational models [25] at sufficiently large times. We remark that our analysis is limited due to finite size effect at long times, thus we do not observe such transient behavior in the global MSD. A detailed analysis of this limitation is discussed in Appendix A.

The presented RWPT model here is able to accurately model bacterial transport in confined porous media in an effective way. Our RWPT model differs from previous modeling attempts using two transport modes, which neglect the angular distribution in the trapping mode and only use the two preferred turning angles in this mode to model cell transport [5, 31]. Most importantly, our proposed approach provides means to define a quantitative measure to understand the transition spectrum between hopping and trapping modes and its impact on different variations of trajectory.

IV. CONCLUSIONS

We use pattern recognition techniques in a direct visualization of bacterial migration to extract statistical parameters used as input for the trajectory simulations. The analysis of turn-angle distributions in combination with speed shows coupling, which suggest directional persistence in bacteria trajectories. This means that when cells are moving fast the probability of staying in a directed path through the pore space is high. Moreover, when cells encounter a trap they reorient its body until it is able to escape with almost uniform distribution of speed. Inspection of the transport dynamics shows that for both hopping and trapping modes, the Gamma distribution fits the marginal velocity best, while an ex-

ponential distribution shows that describes well the hopping and trapping-time distributions when used as an approximation. These observations thus contradict the paradigm of run-and-tumble motility which traditionally is assumed to persist in a porous medium [1], and clarifies the impact of porous media confinement on bacteria motility.

Our RWPT model describes well the transport dynamics of motile bacteria observed in the experimental visualization analyzed as it takes into account the constraints imposed by the device itself and its obstacles, as well as cell-cell collisions, which may induce the subdiffusive behavior observed in the smaller pore size. Moreover, the model provides a good description of the observed MSD and velocity autocorrelation functions. This is a further justification that the RWPT approach is appropriate to describe the motility patterns of *E. coli* in confined porous media. The approach used imposes no statistical restrictions on the stochastic processes representing bacterial spatial random increments. Each particle moves based on alternating motility states based on the information extracted from the trajectory analysis, and Brownian diffusion.

The RWPT framework used can also provide a systematic approach to extract knowledge and insights of bacteria motility that leads to a better understanding of bacteria behavior at larger scales.

V. ACKNOWLEDGEMENTS

L.P., R.P. and N.S. work was financially supported by U.S. Department of Energy (DOE) grant DESC0019437. L.P. acknowledges the support of the Desert Research Institute (DRI) through the Post Doc Support (PG19123). Work by T.B. and S.S.D. was supported by NSF grant CBET-1941716, the Project X Innovation Fund, a distinguished postdoctoral fellowship from the Andlinger Center for Energy and the Environment at Princeton University to T.B., and in part by funding from the Princeton Center for Complex Materials, a Materials Research Science and Engineering Center supported by NSF grant DMR-1420541.

Appendix A: Finite size effects on experimetal data

We illustrate here the full evolution of the experimental global MSD which suggests a late diffusive regime arises after the subdiffusive behavior. However, at these long times where the transition is expected to occur, we lost $\sim 30\%$ of the cells tracked for $\lambda = 1.9\mu$m and $\sim 25\%$ for $\lambda = 3.6\mu$m, such data reduction affects the MSD observed and consequently noisy data appear. This limitation prevent us to claim that the subdiffusive behavior is transient and collapses back to normal diffusion. On the other hand, the model captures such subdiffusion transiency and predicts a diffusive regime at $t \gg \tau_h$, however the crossover time at which our RWPT converges to the diffusive behavior cannot be verified against our experimental data.

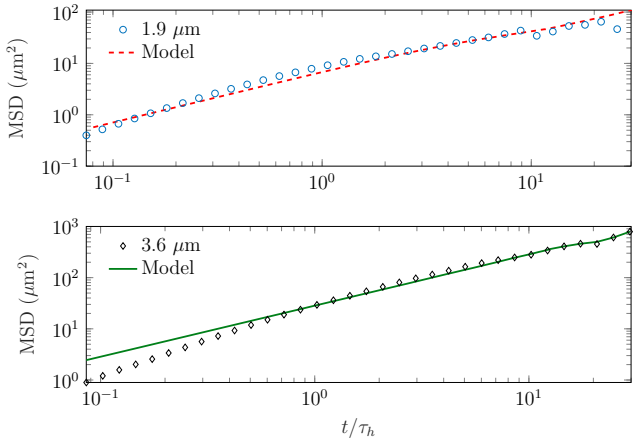

FIG. 9. Full evolution of the mean squared displacement (MSD) computed for different pore sizes, 1.9 μm (upper plot) and 3.6 μm (lower plot). Experimental MSD is shown in symbols in both plots, and the RWPT simulation results for 1.9 μm (red dashed line in upper plot) and 3.6 μm (green solid line in lower plot).

[1] P. S. Lovely and F. Dahlquist, Statistical measures of bacterial motility and chemotaxis, Journal of theoretical biology **50**, 477 (1975).
[2] R. Singh, D. Paul, and R. K. Jain, Biofilms: implications in bioremediation, Trends in microbiology **14**, 389 (2006).
[3] S. J. Edwards and B. V. Kjellerup, Applications of biofilms in bioremediation and biotransformation of persistent organic pollutants, pharmaceuticals/personal care products, and heavy metals, Applied microbiology and biotechnology **97**, 9909 (2013).
[4] J. Song, Y. Zhang, C. Zhang, X. Du, Z. Guo, Y. Kuang, Y. Wang, P. Wu, K. Zou, L. Zou, *et al.*, A microfluidic device for studying chemotaxis mechanism of bacterial cancer targeting, Scientific reports **8**, 1 (2018).
[5] J. Taktikos, H. Stark, and V. Zaburdaev, How the motility pattern of bacteria affects their dispersal and chemotaxis, PloS one **8** (2013).
[6] D. Scheidweiler, F. Miele, H. Peter, T. J. Battin, and P. de Anna, Trait-specific dispersal of bacteria in heterogeneous porous environments: from pore to porous medium scale, Journal of the Royal Society Interface **17**, 20200046 (2020).
[7] P. D. Frymier, R. M. Ford, H. C. Berg, and P. T. Cummings, Three-dimensional tracking of motile bacteria near a solid planar surface, Proceedings of the National Academy of Sciences **92**, 6195 (1995).

[8] G. Li, L.-K. Tam, and J. X. Tang, Amplified effect of brownian motion in bacterial near-surface swimming, Proceedings of the National Academy of Sciences **105**, 18355 (2008).

[9] X. Yang, R. Parashar, N. L. Sund, A. E. Plymale, T. D. Scheibe, D. Hu, and R. T. Kelly, On modeling ensemble transport of metal reducing motile bacteria, Scientific reports **9**, 1 (2019).

[10] L. Xie, T. Altindal, S. Chattopadhyay, and X.-L. Wu, Bacterial flagellum as a propeller and as a rudder for efficient chemotaxis, Proceedings of the National Academy of Sciences **108**, 2246 (2011).

[11] V. Arabagi, B. Behkam, E. Cheung, and M. Sitti, Modeling of stochastic motion of bacteria propelled spherical microbeads, Journal of Applied Physics **109**, 114702 (2011).

[12] C. E. López, A. Théry, and E. Lauga, A stochastic model for bacteria-driven micro-swimmers, Soft matter **15**, 2605 (2019).

[13] N. A. Licata, B. Mohari, C. Fuqua, and S. Setayeshgar, Diffusion of bacterial cells in porous media, Biophysical journal **110**, 247 (2016).

[14] F. Detcheverry, Generalized run-and-turn motions: From bacteria to lévy walks, Physical Review E **96**, 012415 (2017).

[15] X. Liang, N. Lu, L.-C. Chang, T. H. Nguyen, and A. Massoudieh, Evaluation of bacterial run and tumble motility parameters through trajectory analysis, Journal of contaminant hydrology **211**, 26 (2018).

[16] G. Danuser, J. Allard, and A. Mogilner, Mathematical modeling of eukaryotic cell migration: insights beyond experiments, Annual review of cell and developmental biology **29**, 501 (2013).

[17] R. S. Marken and W. T. Powers, Random-walk chemotaxis: Trial and error as a control process., Behavioral neuroscience **103**, 1348 (1989).

[18] L. Xie, T. Altindal, and X.-L. Wu, An element of determinism in a stochastic flagellar motor switch, PloS one **10**, e0141654 (2015).

[19] F. Safaeifard, S. P. Shariatpanahi, and B. Goliaei, A survey on random walk-based stochastic modeling in eukaryotic cell migration with emphasis on its application in cancer, Multidisciplinary Cancer Investigation **2**, 1 (2018).

[20] W. Alt, Biased random walk models for chemotaxis and related diffusion approximations, Journal of mathematical biology **9**, 147 (1980).

[21] H. Karani, G. E. Pradillo, and P. M. Vlahovska, Tuning the random walk of active colloids: From individual run-and-tumble to dynamic clustering, Physical review letters **123**, 208002 (2019).

[22] R. Parashar, D. OMalley, and J. H. Cushman, Mean first-passage time for superdiffusion in a slit pore with sticky boundaries, Physical Review E **78**, 052101 (2008).

[23] R. Parashar and J. H. Cushman, Scaling the fractional advective–dispersive equation for numerical evaluation of microbial dynamics in confined geometries with sticky boundaries, Journal of Computational Physics **227**, 6598 (2008).

[24] T. Marquez-Lago, A. Leier, and K. Burrage, Anomalous diffusion and multifractional brownian motion: simulating molecular crowding and physical obstacles in systems biology, IET systems biology **6**, 134 (2012).

[25] F. Höfling and T. Franosch, Anomalous transport in the crowded world of biological cells, Reports on Progress in Physics **76**, 046602 (2013).

[26] B. ten Hagen, S. van Teeffelen, and H. Löwen, Brownian motion of a self-propelled particle, Journal of Physics: Condensed Matter **23**, 194119 (2011).

[27] T. Bhattacharjee and S. S. Datta, Bacterial hopping and trapping in porous media, Nature communications **10**, 2075 (2019).

[28] T. Bhattacharjee and S. S. Datta, Confinement and activity regulate bacterial motion in porous media, Soft Matter **15**, 9920 (2019).

[29] J. C. Crocker and D. G. Grier, Methods of digital video microscopy for colloidal studies, Journal of colloid and interface science **179**, 298 (1996).

[30] M. Theves, J. Taktikos, V. Zaburdaev, H. Stark, and C. Beta, A bacterial swimmer with two alternating speeds of propagation, Biophysical journal **105**, 1915 (2013).

[31] E. V. Pankratova, A. I. Kalyakulina, M. I. Krivonosov, S. V. Denisov, K. M. Taute, and V. Y. Zaburdaev, Chemotactic drift speed for bacterial motility pattern with two alternating turning events, PloS one **13** (2018).

[32] J. Taktikos, V. Zaburdaev, and H. Stark, Modeling a self-propelled autochemotactic walker, Physical Review E **84**, 041924 (2011).

[33] J. E. Sosa-Hernández, M. Santillán, and J. Santana-Solano, Motility of escherichia coli in a quasi-two-dimensional porous medium, Physical Review E **95**, 032404 (2017).

[34] L. J. Perez, J. J. Hidalgo, and M. Dentz, Reactive random walk particle tracking and its equivalence with the advection-diffusion-reaction equation, Water Resources Research **55**, 847 (2019).

[35] A. Puyguiraud, L. J. Perez, J. J. Hidalgo, and M. Dentz, Effective dispersion coefficients for the upscaling of pore-scale mixing and reaction, Advances in Water Resources **146**, 103782 (2020).

[36] G. Marsaglia and W. W. Tsang, A simple method for generating gamma variables, ACM Transactions on Mathematical Software (TOMS) **26**, 363 (2000).

[37] L. Martino and J. Míguez, A generalization of the adaptive rejection sampling algorithm, Statistics and Computing **21**, 633 (2011).

[38] S. G. Nurzaman, Y. Matsumoto, Y. Nakamura, K. Shirai, S. Koizumi, and H. Ishiguro, From lévy to brownian: a computational model based on biological fluctuation, PloS one **6** (2011).

[39] M. R. Shaebani and H. Rieger, Transient anomalous diffusion in run-and-tumble dynamics, Frontiers in Physics **7**, 120 (2019).

[40] S. Engblom, P. Lötstedt, and L. Meinecke, Mesoscopic modeling of random walk and reactions in crowded media, Physical Review E **98**, 033304 (2018).

[41] T. Kaya and H. Koser, Direct upstream motility in escherichia coli, Biophysical journal **102**, 1514 (2012).

[42] J. Taktikos, V. Zaburdaev, and H. Stark, Collective dynamics of model microorganisms with chemotactic signaling, Physical Review E **85**, 051901 (2012).

[43] L. Turner, W. S. Ryu, and H. C. Berg, Real-time imaging of fluorescent flagellar filaments, Journal of bacteriology **182**, 2793 (2000).

[44] L. Cisneros, C. Dombrowski, R. E. Goldstein, and J. O. Kessler, Reversal of bacterial locomotion at an obstacle,

Physical Review E **73**, 030901 (2006).
[45] S. Bianchi, F. Saglimbeni, A. Lepore, and R. Di Leonardo, Polar features in the flagellar propulsion of e. coli bacteria, Physical Review E **91**, 062705 (2015).
[46] G. J. McLachlan and D. Peel, *Finite mixture models* (John Wiley & Sons, 2004).
[47] K. Taute, S. Gude, S. Tans, and T. Shimizu, High-throughput 3d tracking of bacteria on a standard phase contrast microscope, Nature communications **6**, 1 (2015).
[48] P. L. Irwin, L.-H. T. Nguyen, G. C. Paoli, and C.-Y. Chen, Evidence for a bimodal distribution of escherichia coli doubling times below a threshold initial cell concentration, BMC microbiology **10**, 207 (2010).
[49] K. J. Duffy, P. T. Cummings, and R. M. Ford, Random walk calculations for bacterial migration in porous media, Biophysical journal **68**, 800 (1995).
[50] K. J. Duffy and R. M. Ford, Turn angle and run time distributions characterize swimming behavior for pseudomonas putida., Journal of bacteriology **179**, 1428 (1997).
[51] A. Creppy, E. Clément, C. Douarche, M. V. d'Angelo, and H. Auradou, Effect of motility on the transport of bacteria populations through a porous medium, Physical Review Fluids **4**, 013102 (2019).
[52] E. M. Calvo-Muñoz, M. E. Selvan, R. Xiong, M. Ojha, D. J. Keffer, D. M. Nicholson, and T. Egami, Applications of a general random-walk theory for confined diffusion, Physical Review E **83**, 011120 (2011).
[53] S. C. Weber, M. A. Thompson, W. E. Moerner, A. J. Spakowitz, and J. A. Theriot, Analytical tools to distinguish the effects of localization error, confinement, and medium elasticity on the velocity autocorrelation function, Biophysical journal **102**, 2443 (2012).
[54] R. Metzler, J.-H. Jeon, and A. Cherstvy, Non-brownian diffusion in lipid membranes: Experiments and simulations, Biochimica et Biophysica Acta (BBA)-Biomembranes **1858**, 2451 (2016).
[55] M. A. Desposito and A. D. Viñales, Subdiffusive behavior in a trapping potential: mean square displacement and velocity autocorrelation function, Physical Review E **80**, 021111 (2009).
[56] M. Weiss, M. Elsner, F. Kartberg, and T. Nilsson, Anomalous subdiffusion is a measure for cytoplasmic crowding in living cells, Biophysical journal **87**, 3518 (2004).